JACS
JOURNAL OF THE AMERICAN CHEMICAL SOCIETY

Communication

pubs.acs.org/JACS

Low Temperature Growth of Highly Nitrogen-Doped Single Crystal Graphene Arrays by Chemical Vapor Deposition

Yunzhou Xue,‡ Bin Wu,‡ Lang Jiang, Yunlong Guo, Liping Huang, Jianyi Chen, Jiahui Tan, Dechao Geng, Birong Luo, Wenping Hu, Gui Yu, and Yunqi Liu*

Beijing National Laboratory for Molecular Sciences, Institute of Chemistry, Chinese Academy of Sciences, Beijing 100190, P. R. China

Supporting Information

ABSTRACT: The ability to dope graphene is highly important for modulating electrical properties of graphene. However, the current route for the synthesis of N-doped graphene by chemical vapor deposition (CVD) method mainly involves high growth temperature using ammonia gas or solid reagent melamine as nitrogen sources, leading to graphene with low doping level, polycrystalline nature, high defect density and low carrier mobility. Here, we demonstrate a self-assembly approach that allows the synthesis of single-layer, single crystal and highly nitrogen-doped graphene domain arrays by self-organization of pyridine molecules on Cu surface at temperature as low as 300 °C. These N-doped graphene domains have a dominated geometric structure of tetragonal-shape, reflecting the single crystal nature confirmed by electron-diffraction measurements. The electrical measurements of these graphene domains showed their high carrier mobility, high doping level, and reliable N-doped behavior in both air and vacuum.

Graphene, a two-dimensional (2D) monolayer form of sp^2-hybridized carbon atoms, has attracted wide-ranging interests in both fundamental and applied scientific researches since it was discovered in 2004.[1] Various potential applications based on its excellent mobility of both electron and hole require a reliable synthesis route for the production of high quality graphene materials. Several methods including mechanical cleave,[1] chemical treatments of graphite,[2−4] solvothermal method,[5,6] and the more recent and popular chemical vapor deposition (CVD) method[7−13] have been demonstrated to be useful for certain purposes. These achievements showed that various building blocks ranging from C atoms, molecules,[14] and graphite[15] can be used to produce the final graphene with different formation mechanisms. Especially, self-organization into graphene lattice from atoms or molecules is interesting as it allows the potential manipulations of graphene morphology (related to internal crystalline structures), element doping (n- or p-type) for tuning its electrical properties and geometric parameters by controlling the related conditions.

A few works have been focused on the synthesis of N-doped graphene[16−23] and single crystal pristine graphene[24−28] with different morphologies at high growth temperature (900−1000 °C) using CVD method. However, high temperature process leads to several problems in the case of N-doping such as insufficient doping of graphene, increased defect density in lattice, polycrystalline nature, and low device performance. For example, the doping level in graphene with N element is a critical parameter which determines the n-type behavior in ambient condition as graphene is p-type with adsorbed oxygen in air. However, higher doping level of nitrogen in graphene is difficult to realize as N source also needs to breakdown into N atoms at high temperature before incorporating into graphene lattice, no matter if ammonia gas or solid doping reagent melamine was used. In general, the process of doping is a competition between the formation of C−C and C−N networks to achieve the minimum internal energy. This competition is expected to be strongly affected by temperature, that is, higher temperature favors the C−C bond formation, thus possibly suppressing N doping.[17] On the basis of the above consideration, a low temperature synthesis technique is highly desirable to grow high N content graphene, and it is also environment-friendly and economical for the large-scale production in industry. Direct self-organization into graphene from N-contained molecules without dissociation may provide an approach to grow N-doped graphene in a controlled manner.

Here, we report a large-scale synthesis of highly N-doped tetragonal-shaped single crystal graphene (NTSG) arrays via a self-assembly of pyridine molecules on Cu surface by an ambient pressure CVD method at 300 °C, which is the lowest temperature reported to date for growing N-doped graphene. This approach allows the growth of almost 100% single-layer, single crystal structure graphene domains with unique tetragonal-shape. The N atoms arranged in every hexahydric ring of the graphene, with N content of 16.7% that is much higher than the previous obtained N-doped graphene. The evaluation of NTSG electrical properties revealed the reliable N-doped characteristics in both air and vacuum conditions and remarkable high electron mobility of 53.6−72.9 $cm^2/V{\cdot}s$, which is higher than those produced by high temperature CVD method.[16,17,22]

As schematically shown in Figure 1a, the self-assembly into graphene structure by pyridine molecules involves the adsorption on Cu surface, and then hexahydric ring dehydrogenates at low temperature (note that the dehydrogenation temperature of pyridine molecules is much lower than the hexahydric ring decomposition temperature of pyridine (620−

Received: March 14, 2012
Published: June 22, 2012

   dx.doi.org/10.1021/ja302483t | J. Am. Chem. Soc. 2012, 134, 11060−11063

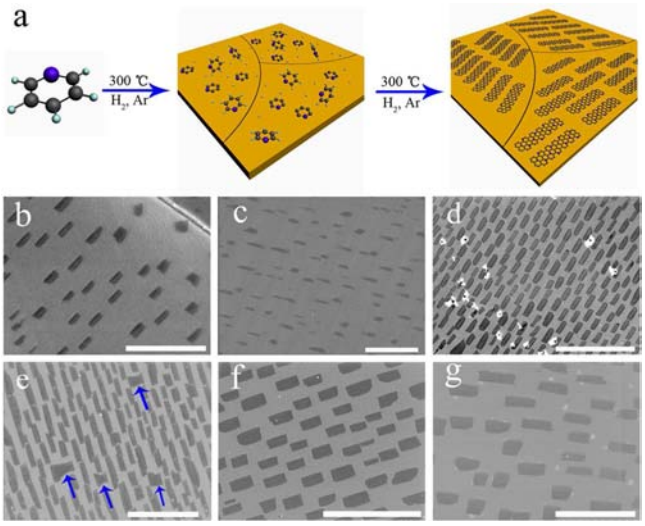

Figure 1. (a) Schematic diagram of the NTSGs growth on a copper surface with pyridine as both the carbon and nitrogen sources by CVD at ambient pressure, where gray balls represent C atoms, purple for N atoms, and light green for hydrogen atoms. (b–g) SEM images of NTSGs on copper surface under different conditions, respectively (see also Table S1). The blue arrows in panel e indicate that two different graphene domains combine together at this experiment conditions. All scale bars are 5 μm.

650 °C)).[29] These building blocks are energetically active to organize themselves into ordered structures by surface diffusion, being similar to the process of common CVD process involving C atoms. Figure 1b–g and Figure S1 show the typical scanning electron microscopy (SEM) images of NTSGs grown on Cu surface by bubbling liquid pyridine with hydrogen and argon as the carrier gas at ambient pressure under different conditions (see Table S1). The NTSG domains were uniformly grown on the Cu surface and exhibited tetragonal shape with aspect ratio about 2–5 in a very high yield. The size distribution was relatively narrow with average values of 1–2 μm in the long direction of tetragonal-shaped graphene. As the growth time was increased from 0.5 min (Figure 1b), 1 min (Figure 1c), 3 min (Figure 1d) to 5 min (Figure 1e), both densities and sizes of graphene domains increased. Decreasing overall flow rate of carrier gas led to slower nucleation and growth as shown in Figure 1f,g. These results are excellently consistent with the general phenomena of graphene grown on Cu surface via nucleation and growth mechanism; that is, the nucleation and growth are competing processes during growth. The graphene size and density reflect the characteristics in terms of the ease of pyridine molecule nucleation, surface diffusion rate, and corresponding changes at the experimental conditions in this special system.

These observations show a remarkable analogy to the cases of using CH_4 as a carbon precursor to produce single crystal graphene with a unique shape of hexagon graphene on Cu surface at 1000 °C[24−27] or rectangular-shaped graphene domains on Cu (111) grains at 980 °C.[28] There is no clear orientation among different domains observed as explained by weak epitaxial interactions between graphene and Cu surface. In contrast, the use of larger pyridine molecules results in the formation of graphene domains with different well-defined shapes. Interestingly, the NTSGs appeared to align on a single Cu grain (Figure 1b–g) and this alignment is also evident when two disoriented Cu grains are separated by a clear grain boundary as shown in Figure S2. The good alignment observed on all Cu grains in our results has no connection with the gas flow direction, and is supposed to be related to the underlying Cu surface lattice structure. This is understandable because low temperature used in our case leads to low thermal energy of adsorbed pyridine molecules, thus making the interactions stronger between molecules and Cu lattice.[28] This consideration may account for the less alignment of graphene domains on Cu surface grown at high temperature.[24,27] The formation of high aspect ratio NTSGs is also consistent with the above analysis, since the strong anisotropic interactions between graphene and Cu lattice produces a different growth rate along different directions.

To evaluate the quality of the NTSGs, Raman spectroscopy was used with the laser at 633 nm excitation wavelength. The three most pronounced peaks in the spectrum, the D band, a first-order zone boundary phonon mode associated with defects in the graphene or graphene edge; G band, a radial C–C stretching mode of sp^2 bonded carbon; and 2D band, a second-order zone boundary phonon mode for graphene and graphite appeared at 1325, 1586, and 2638 cm^{-1}, respectively (Figure 2a). The weak D band indicates low density of defects and the

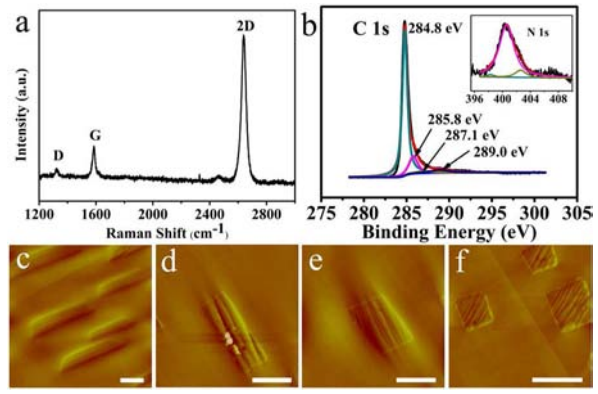

Figure 2. (a) Raman spectra (633 nm laser wavelength) of NTSGs on a copper surface. (b) XPS spectra of NTSGs on copper surfaces. (c–f) AFM images of different tetragonal-shaped morphologies for isosceles trapezoid, rectangle, parallelogram and square, respectively. All scale bars are 1 μm.

intensity ratio of D band and G band (I_D/I_G) reflects the degree of the defects in the graphene or the edges. Typically, the nitrogen insertions in the sp^2 carbon introduce topological defects,[16] thus increasing the I_D/I_G ratio. In our NTSG samples, the I_D/I_G is about 0.16 that is much lower than the typical value of 0.3–0.4 for the polycrystalline N-doped graphene[16] produced by high temperature CVD, indicating much reduced defect density of our single crystal structure. As is well-known, the 2D band is the most prominent feature in the Raman spectra of graphene; its shape and intensity are very sensitive to the number of layers. For single-layer graphene, the 2D band is a single, sharp, and symmetric peak. In Figure 2a, the 2D band is a symmetric peak with a full width at half-maximum (fwhm) of 38 cm^{-1}, which is in accordance with the parameters for the single-layer graphene as the bilayer and few-layer graphene have broader 2D band than the single-layer graphene. Meanwhile, the intensity ratio of G band and 2D band (I_G/I_{2D}) is well established to characterize the graphene layers. The I_G/I_{2D} in Figure 2a is about 0.21, which is a characteristic of single-layer graphene. In addition, uniform contrast in SEM images of

dx.doi.org/10.1021/ja302483t | J. Am. Chem. Soc. 2012, 134, 11060–11063

Figure 1b–g also strongly indicates the single-layer nature. Statistically, Raman spectra for all measured NTSGs (Figure S3a) and AFM height measurement (Figure S3b) for transferred NTSGs show single-layer characteristics. High selectivity of producing single-layer graphene is not sensitive to the parameters we adopted. This may be due to the fact that the pyridine molecules take part in reaction as an intact hexahydric ring, and it is not easy for several hexahydric rings to form a new critical nucleation center below or above the first grown layer possibly due to the limited diffusion.

X-ray photoelectron spectroscopy (XPS) was performed on copper surface to detect the N doping level in graphene as shown in Figure 2b. The main C 1s peak located at 284.8 eV corresponds to the graphite-like sp^2 C. The other three small peaks are located at 285.8, 287.1, and 289.0 eV, reflecting two different C–N bonding structures with sp^2- and sp^3- hybridized carbon and C–O bonding structure, respectively.[17] The clear N 1s peak is observed, confirming the existence of N doping element (Figure 2b, inset). The asymmetric N 1s peak can be divided into three components located at 398.3, 400.7, and 402.6 eV, which correspond to pyridine, graphitic, and oxidized nitrogen,[19,30,31] respectively. The estimation of N doping level is lower than the expected value. This difference is reasonable as C adsorption on Cu surface from ambient environment is almost unavoidable. Control experiments indeed show the existence of C 1s peak at 284.8 eV in XPS measurement on bare Cu foil without graphene growth as shown in Figure S5.

Atomic force microscopy (AFM) was used to further probe the detailed morphology of NTSG domains. Figure 2c–f shows the AFM images of four different morphologies graphene domains for isosceles trapezoid, rectangle, parallelogram, and square on the copper substrate, respectively. These shaped domains share common features in that two straight edges are parallel to each other with the other two edges adopted with different angles. The AFM images also show wrinkled or rippled structures on the graphene surface (see also Figure S4), which is most likely caused by Cu contraction due to the different thermal expansion coefficients of graphene and copper substrate during cooling process, consistent with the previous observation.[24]

The perfection of graphene lattice structure of the obtained tetragonal-shaped graphene was studied by transmission electron microscopy (TEM), and the image and diffraction patterns are shown in Figure 3. The profile of the tetragonal-shape can be clearly identified and appear as homogeneous and featureless regions in Figure 3a, whereas the membranes' edges tend to scroll. The selected area electron diffraction (SAED) patterns in Figure 3b display the typical hexagonal crystalline structure of graphene at different regions marked **1**–**5** in Figure 3a. The same 6-fold symmetric diffraction spots at five different places indicate that the tetragonal-shaped N-doped graphene is a single crystalline material. Other four different graphene domains were also characterized by SAED and were all confirmed as single crystal (Figure S6). The SAED images in Figure 3b and Figure S6 also confirm that the graphene domains are single-layer since the {1100} six spots appear to be intense relative to the {2110} spots.[32] Figure 3c shows the higher resolution TEM image of the folded edge from the region indicated with the white arrow in Figure 3a, further confirming that the graphene is single layer.

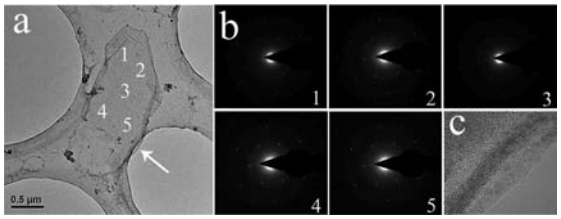

Figure 3. (a) TEM image of NTSG and (b) the corresponding SAED on the regions marked by numbers in (a), respectively. (c) High resolution TEM image corresponding to the region marked by white arrow in (a) showing single layer.

To further evaluate the quality and electrical property of the obtained NTSGs, NTSG-based back-gate field-effect transistors (FETs) were fabricated on a 500 nm SiO_2/Si substrate with Au as the source/drain electrodes and the doped silicon as the back gate. The details for the device fabrication process are provided in Supporting Information.[33] Figure 4a,b demonstrates the electrical properties of a typical NTSG-based device measured in air at room temperature. The inset in Figure 4b shows a SEM image of an as-made device. As is seen in Figure 4b, the Dirac point of our NTSG device remarkably shifted to negative gate voltage (~−26 V), demonstrating an typical n-type electron doping performance. In contrast, most of the reported N-doped graphene did not exhibit n-type performance in air, and n-type behavior is only realized by measurements performed under vacuum due to the removal of adsorbents from the graphene surface.[16,17,22] This fact indicates the low N content in their N-doped graphene sample so that the adsorbents on graphene surface such as O_2 and H_2O effectively neutralize their n-type feature in air. Further electrical measurements of our sample under vacuum (chamber pressure: ~10^{-3} Pa) showed the expected shift of transfer curve toward negative gate voltage, leading to the absence of Dirac point down to ~−60 V. This result is well consistent with the high N-doping level in our sample. The measured mobility of our NTSG FET devices were found in the range of 53.5–72.9 $cm^2\ V^{-1}\ s^{-1}$, which were much higher than many of the N-doped graphene prepared by CVD method reported previously,[16,17,22] reflecting the good

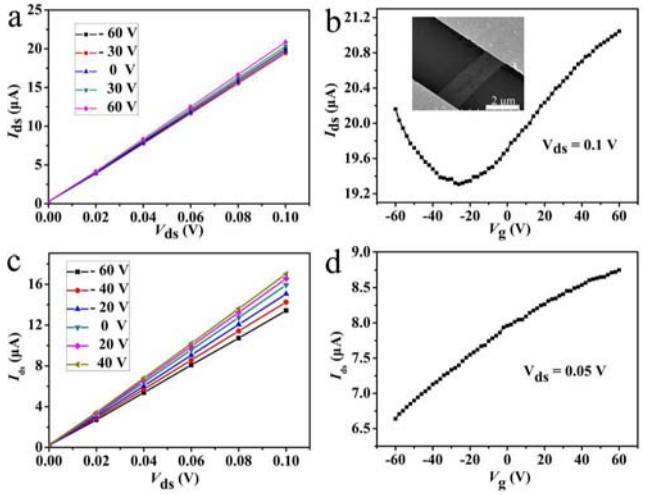

Figure 4. Electrical properties of NTSGs: (a) I_{ds}/V_{ds} characteristics at various V_g and (b) transfer characteristics of the NTSG in air, with the neutrality point at ~−26 V. The inset shows a top view SEM image of the NTSG device. (c) I_{ds}/V_{ds} characteristics at various V_g and (d) transfer characteristics of the NTSG in vacuum, without the neutrality point appeared even at ~−60 V, proving the high nitrogen content.

dx.doi.org/10.1021/ja302483t | J. Am. Chem. Soc. 2012, 134, 11060–11063

quality of our NTSG lattice. Note that the high-doping level generally leads to the reduced mobility. For example, the NTSG mobility is lower than those for edge N-doped graphene nanoribbon by e-annealing technique[34] and CVD-produced pristine graphene[24] due to the carrier scattering by doping atoms.[22]

In summary, we have demonstrated a rational route that allows the synthesis of single-layer, single crystal, tetragonal-shaped, N-doped graphene domain arrays based on self-assembly of pyridine molecules on Cu surface at as low as 300 °C at ambient pressure. The tetragonal-shaped graphene domains show the same aligned direction within a single copper grain. The electrical measurement confirms the typical n-type FETs for N-doped graphene both in air and vacuum, and the mobilities are in the range of 53.5−72.9 $cm^2 V^{-1} s^{-1}$, much higher than those of the N-doped graphene reported. The NTSG is expected to find its unique applications for electronic devices.

■ ASSOCIATED CONTENT

Supporting Information

Experimental procedures and additional figures. This material is available free of charge via the Internet at http://pubs.acs.org.

■ AUTHOR INFORMATION

Corresponding Author

liuyq@iccas.ac.cn

Author Contributions

‡These authors contributed equally.

Notes

The authors declare no competing financial interest.

■ ACKNOWLEDGMENTS

This work was supported by the National Basic Research Program of China (2011CB932700, 2011CB808403, 2011CB932303), the National Natural Science Foundation of China (61171054, 20973184, 20825208, 60911130231), and the Chinese Academy of Sciences.

■ REFERENCES

(1) Novoselov, K. S.; Geim, A. K.; Morozov, S. V.; Jiang, D.; Zhang, Y.; Dubonos, S. V.; Grigorieva, I. V.; Firsov, A. A. *Science* **2004**, *306*, 666.

(2) Park, S.; Ruoff, R. S. *Nat. Nanotechnol.* **2009**, *4*, 217.

(3) Tung, V. C.; Allen, M. J.; Yang, Y.; Kaner, R. B. *Nat. Nanotechnol.* **2009**, *4*, 25.

(4) Gilje, S.; Han, S.; Wang, M.; Wang, K. L.; Kaner, R. B. *Nano Lett.* **2007**, *7*, 3394.

(5) Choucair, M.; Thordarson, P.; Stride, J. A. *Nat. Nanotechnol.* **2009**, *4*, 30.

(6) Deng, D. H.; Pan, X. L.; Yu, L.; Cui, Y.; Jiang, Y. P.; Qi, J.; Li, W. X.; Fu, Q.; Ma, X. C.; Xue, Q. K.; Sun, G. Q.; Bao, X. H. *Chem. Mater.* **2011**, *23*, 1188.

(7) Kim, K. S.; Zhao, Y.; Jang, H.; Lee, S. Y.; Kim, J. M.; Kim, K. S.; Ahn, J. H.; Kim, P.; Choi, J. Y.; Hong, B. H. *Nature* **2009**, *457*, 706.

(8) Sutter, P. W.; Flege, J. I.; Sutter, E. A. *Nat. Mater.* **2008**, *7*, 406.

(9) Li, X. S.; Cai, W. W.; An, J.; Kim, S.; Nah, J.; Yang, D. X.; Piner, R.; Velamakanni, A.; Jung, I.; Tutuc, E.; Banerjee, S. K.; Colombo, L.; Ruoff, R. S. *Science* **2009**, *324*, 1312.

(10) Xue, Y. Z.; Wu, B.; Guo, Y. L.; Huang, L. P.; Jiang, L.; Chen, J. Y.; Geng, D. C.; Liu, Y. Q.; Hu, W. P.; Yu, G. *Nano Res.* **2011**, *4*, 1208.

(11) Wei, D. C.; Liu, Y. Q.; Zhang, H. L.; Huang, L. P.; Wu, B.; Chen, J. Y.; Yu, G. *J. Am. Chem. Soc.* **2009**, *131*, 11147.

(12) Reina, A.; Jia, X. T.; Ho, J.; Nezich, D.; Son, H.; Bulovic, V.; Dresselhaus, M. S.; Kong, J. *Nano Lett.* **2009**, *9*, 30.

(13) Chen, J. Y.; Wen, Y. G.; Guo, Y. L.; Wu, B.; Huang, L. P.; Xue, Y. Z.; Geng, D. C.; Wang, D.; Yu, G.; Liu, Y. Q. *J. Am. Chem. Soc.* **2011**, *133*, 17548.

(14) Li, Z. C.; Wu, P.; Wang, C. X.; Fan, X. D.; Zhang, W. H.; Zhai, X. F.; Zeng, C. G.; Li, Z. Y.; Yang, J. L.; Hou, J. G. *ACS Nano* **2011**, *5*, 3385.

(15) Kwak, J.; Chu, J. H.; Choi, J. K.; Park, S. D.; Go, H.; Kim, S. Y.; Park, K.; Kim, S. D.; Kim, Y. W.; Yoon, E.; Kodambaka, S.; Kwon, S. Y. *Nat. Commun.* **2012**, *3*, 645.

(16) Jin, Z.; Yao, J.; Kittrell, C.; Tour, J. M. *ACS Nano* **2011**, *5*, 4112.

(17) Zhang, C. H.; Fu, L.; Liu, N.; Liu, M. H.; Wang, Y. Y.; Liu, Z. F. *Adv. Mater.* **2011**, *23*, 1020.

(18) Qu, L. T.; Liu, Y.; Baek, J. B.; Dai, L. M. *ACS Nano* **2010**, *4*, 1321.

(19) Reddy, A. L. M.; Srivastava, A.; Gowda, S. R.; Gullapalli, H.; Dubey, M.; Ajayan, P. M. *ACS Nano* **2010**, *4*, 6337.

(20) Luo, Z. Q.; Lim, S.; Tian, Z.; Shang, J. Z.; Lai, L. F.; MacDonald, B.; Fu, C.; Shen, Z. X.; Yu, T.; Lin, J. Y. *J. Mater. Chem.* **2011**, *21*, 8038.

(21) Imamura, G.; Saiki, K. *J. Phys. Chem. C* **2011**, *115*, 10000.

(22) Sun, Z.; Yan, Z.; Yao, J.; Beitler, E.; Zhu, Y.; Tour, J. M. *Nature* **2010**, *468*, 549.

(23) Usachov, D.; Gruneis, O. V. A.; Haberer, D.; Adamchuk, A. F. V. K.; Preobrajenski, A. B.; Dudin, P.; Barinov, A.; Oehzelt, M.; Laubschat, C.; Vyalikh, D. V. *Nano Lett.* **2011**, *11*, 5401.

(24) Wu, B.; Geng, D. C.; Guo, Y. L.; Huang, L. P.; Xue, Y. Z.; Zheng, J.; Chen, J. Y.; Yu, G.; Liu, Y. Q.; Jiang, L.; Hu, W. P. *Adv. Mater.* **2011**, *23*, 3522.

(25) Robertson, A. W.; Warner, J. H. *Nano Lett.* **2011**, *11*, 1182.

(26) Wu, W.; Jauregui, L. A.; Su, Z. H.; Liu, Z. H.; Bao, J. M.; Chen, Y. P.; Yu, Q. K. *Adv. Mater.* **2011**, *23*, 4898.

(27) Yu, Q. K.; Jauregui, L. A.; Wu, W.; Colby, R.; Tian, J.; Su, Z. H.; Cao, H. L.; Liu, Z. H.; Pandey, D.; Wei, D. G.; Chung, T. F.; Peng, P.; Guisinger, N. P.; Stach, E. A.; Bao, J.; Pei, S. S.; Chen, Y. P. *Nat. Mater.* **2011**, *10*, 443.

(28) Wu, Y. A.; Robertson, A. W.; Schaffel, F.; Speller, S. C.; Warner, J. H. *Chem. Mater.* **2011**, *23*, 4543.

(29) Johns, I. B.; McElhill, E. A.; Smith, J. O. *J. Chem. Eng. Data* **1962**, *7*, 277.

(30) Wu, P.; Qian, Y, D.; Du, P.; Zhang, H.; Cai, C. X. *J. Mater. Chem.* **2012**, *22*, 6402.

(31) Sheng, Z. H.; Shao, L.; Chen, J. J.; Bao, W. J.; Wang, F. B.; Xia, X. H. *ACS Nano* **2011**, *5*, 4350.

(32) Hernandez, Y.; Nicolosi, V.; Lotya, M.; Blighe, F. M.; Sun, Z.; De, S.; McGovern, I. T.; Holland, B.; Byrne, M.; Gun'Ko, Y. K.; Boland, J. J.; Niraj, P.; Duesberg, G.; Krishnamurthy, S.; Goodhue, R.; Hutchison, J.; Scardaci, V.; Ferrari, A. C.; Coleman, J. N. *Nat. Nanotechnol.* **2008**, *3*, 563.

(33) Jiang, L.; Gao, J. H.; Wang, E. J.; Li, H. X.; Wang, Z. H.; Hu, W. P.; Jiang, L. *Adv. Mater.* **2008**, *20*, 2735.

(34) Wang, X. R.; Li, X. L.; Zhang, L.; Yoon, Y.; Weber, P. K.; Wang, H. L.; Guo, J.; Dai, H. J. *Science* **2009**, *324*, 768.